Vol. 78 No. 1 ACTA GEOLOGICA SINICA Feb. 2004 73–82

http://www.geojournals.cn/dzxbcn/ch/index.aspx

Determination of the Neoproterozoic Shicaogou Syn-collisional Granite in the Eastern Qinling Mountains and Its Geological Implications

CHEN Danling, LIU Liang, SUN Yong, ZHANG Anda, ZHANG Chengli, LIU Xiaoming and LUO Jinhai

Key Laboratory of Continental Dynamics, Ministry of Education; Department of Geology, Northwest University, Xi'an, Shaanxi 710069; E-mail: dlchen@nwu.edu.cn

Abstract The Shicaogou granite has been identified as a magnesian (Fe-number=0.71–0.76), calcic to calc-alkalic (MALI=3.84–5.76) and peraluminous (ASI=1.06–1.13) granite of the syn-collisional S-type, with high SiO_2 (>71%), Al_2O_3 (>13%) and Na_2O+K_2O (6.28%–7.33%, equal for NaO_2 and K_2O). Trace element and REE analyses show that the granite is rich in LILE such as of Rb, Sr, Ba and Th, and poor in HFSE like Yb, Y, Zr and Hf. Its Rb/Sr ratio is greater than 1; the contents of Nb and Ta, and the ratio of Nb/Ta as well as the REE geochemical features (e.g. REE abundance, visible fractionation of LREE and HREE and medium to pronounced negative Eu anomalies) are all similar to those of crust-origin, continent-continent syn-collisional granite. Moreover, the granite exhibits almost the same pattern as that of the typical continent-continent syn-collisional granite on the spider diagram and all samples fall within the syn-collisional granite field.

The cathodoluminescence (CL) investigations have revealed that the zircon from the Shicaogou granite represents a typical magmatic product characterized by its colorless, transparent and euhedral crystals, and distinct zoning of oscillatory bands. Residual cores of irregular zircon can be found in a few enhedral grains. Trace element studies of the zircon grains, with high contents of P, Y, Hf, Th, U and REE and high ratios of Th/U, obviously positive Ce anomalies and HREE enrichment compared to LREE, also result in the same conclusion.

The LA-ICP-MS U-Pb isotopic data from 24 spots of 21 zircon grains demonstrate that 20 spots in the oscillatory zone yield an average weighted $^{206}Pb/^{238}U$ age of 925±11 Ma, indicating that the Shicaogou granite was formed in the Neoproterozoic. Combined with other Neoproterozoic syn-collisional granites found in the study area, the present geochronological determination can further reveal that collision-amalgamation events could have occurred among some continental blocks in the Qinling orogenic belt during the Neoproterozoic. This in turn provides an accurate chronological constraint on the Neoproterozoic break-up and convergence in the belt.

Key words: LA-ICP-MS, U-Pb dating, zircon, syn-collisional, S-type granite, geological implication, Shicaogou, eastern Qinling Mountains

1 Introduction

The Qinling (Mountains) is a composite orogenic belt which has undergone a long period of evolution, and as we see today, it mainly exhibits the Paleozoic collisional orogeny along the Shangdan fault and the Mesozoic collision and amalgamation along the Mianlüe fault (Zhang Guowei et al., 1997, 2001; Meng and Zhang, 1999; Yang et al., 2002). It is very important for us to reconstruct the formation, development and evolution of the Qinling orogeny in order to recognize the early geological evolution records in this complicated orogenic belt.

In recently years, more and more evidences indicate that there are records of Neoproterozoic tectono-thermal events in the core portion of the northern Qinling orogenic belt (Li et al., 1991; You et al., 1991; Zhang Hongfei et al., 1993; Zhang Zongqing et al., 1994, 1997; Zhou et al., 1996; Dong et al., 1997; Wang Tao et al., 1998, 2002; Zhang Guowei et al., 2001). It has already attracted the attention of geologists worldwide whether these tectono-thermal events responses of the Rodinian supercontinent event in Qinling and the Chinese continent. The existing Neoproterozoic granites in northern Qinling are mainly the Niujiaoshan granite, Dehe granite, Zhaigen granite and Shangnan granite, of which the former three, having similar petrological and geochemical characteristics and in the same tectonic setting, represent products of the same tectonomagmatic event (Zhang Guowei et al., 2001). These granites have been regarded as representatives of the Neoproterozoic syn-collisional granites in the Qinling orogenic belt (You et al., 1991; Wang Tao et al., 1998, 2002). There are nearly no high-quality geochemical data and accurate isotopic chronological determinations in previous studies on these granites due to the limitation of analytical methods, except for the Niujiaoshan granite, for which systematical geochemical data and relatively accurate U-Pb age are available (Wang Xiaoxia et al., 1997; Wang Tao et al., 1998). The Neoproterozoic Shicaogou syn-collisional S-

type granite reported in this paper is mainly based upon the U-Pb zircon geochronological and geochemical studies, which can provide new evidence for the evolution of the Neoproterozoic granites in the eastern Qinling Mountains. Emphasis will also be placed on the elucidation of the early orogeny process of the Qinling orogenic belt.

2 Geological Setting and Petrology

The northern Qinling orogenic belt is located in the northern part of the Qinling Mountains, sandwiched between the Shangdan fault and the Luonan-Luanchuan-Fangcheng fault. The major geological units include the Qinling Group, the Kuanping Group, the Erlangping ophiolitic mélange and the Danfeng ophiolitic mélange. All these are distributed parallel to one another in a direction of WNW and constitute the main portion of the northern Qinling orogenic belt (Fig. 1).

The Qinling Group, the oldest crystalline basement of the Qinling orogenic belt and distributed on the north side of the Shandan fault, is an intermediate to high-grade metamorphic complex, which is mainly composed of gneisses, amphibolites and marble. Most rocks have experienced amphilolitic-facies metamorphism, and granulite-facies metamorphic rocks can be found locally. The Qinling Group is dated as of the early Proterozoic (2000–2200 Ma) and altered by the Neoproterozoic (1000–800 Ma) and early Paleozoic metamorphism (Pei, 1997; Zhang Guowei et al., 2001). The Danfeng ophilitic mélange belt and the Erlangping ophilitic mélange belt are distributed on the south and north side of the Shangdan fault, respectively. The former makes up the stylolitic structural belt of northern and southern Qinling, and is a product resulting from the closure of the Qinling Paleozoic ocean (Meng and Zhang, 1999), while the latter shows some features of Proterozoic back-arc basin-type igneous and ophiolitic rocks (Sun et al., 1996; Zhang Guowei et al., 2001). The Kuanping Group, lying to the north of the Erlangping Group, is mainly composed of a series of deformed and metamorphosed basic volcanics, detrital rocks and carbonates, with ages ranging from the Meso- to Neo-proterozoic (986–1142 Ma) (Zhang Guowei et al., 2001).

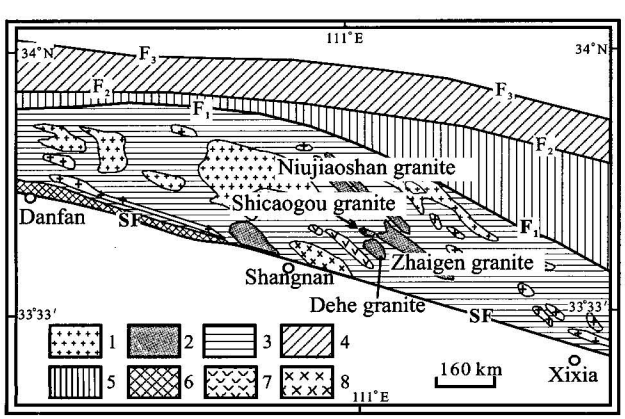

Fig. 1. Geological sketch map of northern Qinling (modified from Wang Tao et al., 2002).
1. Paleozoic granite; 2. Neoproterozoic granite; 3. Qinling Group; 4. Kuanping Group; 5. Erlangping Group; 6. Danfeng Group; 7. Mafic rocks; 8. Gabbro. SF – Shangdan fault; F_1 – Shangxian-Xiaguan fault; F_2 – Huangtai-Waxuezi fault; F_3 – Luonan-Luanchuan-Fangcheng fault.

The Shicaogou granite is situated in the Shicaogou area in Xixia County, Henan Province, on the north side of the Shangdan fault, and about 1–2 km northwest to the Dehe granite body (33°33.682′N, 111°03.649′E; Fig. 1). The granite occurs as a batholith in the Proterozoic Qinling Group gneisses, and displays a strong WNW-directed gneissosisty characterized by elongated quartz and feldspar, which agrees well with trend of the country rock. It is dominated by medium-grained equigranular monzogranite without porphyritic texture, which is different from the Dehe granite but similar to the Zhaigen granite in terms of petrography. The granite body consists mainly of plagioclase (25%–40%), alkili feldspar (25% –40%), quartz (20%–40%), and minor amounts of biotite and muscovite. The accessory minerals include apatite and zircon.

3 Sample Preparation and Analytical Methods

The representative samples (Tables 1 and 2) for this study were analyzed for major and trace elements at the Key Laboratory of Continental Dynamics of the Northwest University, Xi'an, China. The samples for geochemical study were first broken up with a corundum jawbreaker, and then milled using an agate mortar to grains smaller than 0.071 mm. The major element contents, except Fe_2O_3 and LOI analyzed with the wet chemical method, were analyzed using the X-ray fluorescence (RIX2100X sequential spectrometer) on fused Li-borate glass beads. During the analysis, the BCR-2 and GBW07105 standards were used as reference materials. The analytical error for the elements is smaller than 5%. The trace elements and REEs were determined with the ICP-MS (Elan 6100DRC), following the method of Gao et al. (1999). The USGS standards (AGV-1, BCR-1 and BHVO-1) were used for calibration.

Zircon grains for the U-Pb dating were selected from granite samples (about 5 kg in weight), through the batches, heavy liquid and electromagnetic methods, and with binocular microscopes. Dozens of selected colorless and transparent zircon grains were stuck on the double-faced adhesive paper, and then embedded in epoxy and polished to their half sizes when the epoxy is completely solidified.

Table 1 Major element compositions (wt%) and classification parameters of the Shicaogou granite

	SiO_2	TiO_2	Al_2O_3	Fe_2O_3	FeO	MnO	MgO	CaO	Na_2O	K_2O	P_2O_5	LOI	Total	K_2O/Na_2O	P	Q	ACNK	ANK	Fe-number	MALI	ASI
02Q-23	72.18	0.38	13.28	0.55	2.48	0.05	0.87	1.85	2.85	4.13	0.08	0.55	99.53	1.45	−37.25	198.98	1.06	1.45	0.74	5.13	1.07
02Q-24	72.78	0.30	13.73	0.61	1.88	0.05	0.75	1.67	3.07	3.86	0.08	1.00	99.99	1.26	−46.87	203.08	1.12	1.49	0.71	5.26	1.13
02Q-24R	72.68	0.29	13.71	0.60	1.90	0.05	0.75	1.65	3.04	3.87	0.08	1.05	99.88	1.27	−45.33	203.52	1.13	1.49	0.72	5.26	1.13
02Q-25	73.89	0.22	13.45	0.19	1.75	0.04	0.55	1.57	3.71	3.62	0.05	0.37	99.60	0.98	−70.83	194.88	1.04	1.34	0.76	5.76	1.05
02Q-26	72.20	0.34	14.11	0.51	2.35	0.05	0.80	2.36	3.78	2.72	0.08	0.55	100.11	0.72	−106.28	192.96	1.05	1.54	0.75	4.14	1.06
02Q-28	71.81	0.37	14.09	0.46	2.75	0.06	0.92	2.44	3.67	2.61	0.09	0.32	99.90	0.71	−106.49	195.73	1.06	1.59	0.75	3.84	1.07
Niujiaoshan granite	72.85	0.34	13.40	0.91	2.22	0.05	0.74	1.27	3.56	2.86	0.11	1.07	99.38	0.80	−76.77	213.65	1.19	1.50	0.75	5.15	1.20
Dehe granite	70.73	0.20	13.28	1.03	3.27	0.06	1.27	1.90	2.33	3.94	0.15	0.93	99.11	1.69	−25.40	211.14	1.15	1.64	0.72	4.37	1.17

Note: P=[K-(Na+Ca)], Q=[Si/3-(K+Na+2Ca/3)], ACNK=[Al_2O_3/(CaO+Na_2O+K_2O)], ANK=[Al_2O_3/(Na_2O+K_2O)], MALI=K_2O+Na_2O–CaO, ASI=Al/(Ca-1.67P+Na+K). 02Q–24R are the repeated analyses of 02Q-24 to ensure the accuracy of samples; data of the Niujiaoshan granite quoted from Wang Xiaoxia et al. (1997) and those of the Dehe granite from You et al. (1991).

Table 2 Trace element compositions (μg/g) and ratios of the Shicaogou granite

Elements	02Q-23	02Q-24	02Q-25	02Q-26	02Q-28	BHVO-1 analyzed	BHVO-1 referenced	AGV-1 analyzed	AGV-1 referenced
Li	34.2	36.9	19.9	39.3	40.2	5.3	4.6	10.8	12.0
Be	2.31	1.65	2.59	2.40	2.06	1.00	1.10	2.30	2.10
Sc	7.5	6.3	3.9	7.3	8.4	32.5	31.8	12.2	12.2
V	28.3	23.5	17.0	25.4	28.6	325	317	116	121
Cr	16.8	18.0	12.8	34.0	20.0	294	289	10	10
Co	85	88	75	98	83	45	45	15	15
Ni	6.8	7.6	4.9	8.3	7.4	123	121	16	16
Cu	9.1	11.3	11.0	10.7	14.8	144	136	58	60
Zn	42.6	38.0	32.5	38.0	41.7	114	105	82	88
Ga	13.9	13.8	12.6	15.0	15.4	21.2	21.0	19.8	20.0
Ge	1.73	1.54	1.8.0	1.67	1.63	1.7.0	1.64	1.28	1.25
Rb	178.3	205.7	159.7	133.4	126.2	9.1	11.0	64.6	67.3
Sr	60.7	71.5	59.0	100.7	132	405	403	669	662
Y	36.6	28.6	48.6	30.2	40.8	27.5	27.6	20.0	20.0
Zr	142	150	139	177	217	173	179	227	227
Nb	9.2	8.3	7.2	8.9	9.5	18.6	19.0	13.9	15.0
Cs	7.52	8.45	5.76	8.01	7.52	0.10	0.13	1.30	1.28
Ba	457	572	430	463	491	135	139	1232	1226
Hf	4.54	4.43	4.62	5.12	6.31	4.40	4.40	5.10	5.10
Ta	1.66	1.24	1.56	1.45	1.25	1.20	1.20	0.90	0.90
Pb	29.61	31.92	39.12	21.74	24.45	2.0	2.6	38.2	36.0
Th	19.53	19.84	22.12	19.39	20.05	1.20	1.0	6.3	6.5
U	9.43	6.78	9.22	5.62	7.14	0.4	0.4	1.9	1.9
La	32.1	31.5	30.2	34.4	36.9	15.2	15.8	38.3	38.0
Ce	61.7	56.3	54.6	62.1	68.6	36.8	39.0	66.8	67.0
Pr	7.13	6.32	6.3	6.91	7.77	5.34	5.70	8.50	7.60
Nd	26.2	23.0	23.4	25.2	28.8	25.2	25.2	33.0	33.0
Sm	5.45	4.61	5.37	4.89	5.73	6.23	6.20	5.94	5.90
Eu	0.71	0.79	0.59	0.78	0.84	1.95	2.06	1.65	1.64
Gd	5.39	4.48	5.36	4.77	5.64	6.06	6.40	5.33	5.00
Tb	0.93	0.77	1.06	0.80	0.98	0.97	0.96	0.72	0.70
Dy	5.56	4.55	6.77	4.77	5.85	5.23	5.20	3.67	3.60
Ho	1.18	0.96	1.50	1.01	1.23	0.97	0.99	0.69	0.67
Er	3.29	2.72	4.37	2.82	3.43	2.38	2.40	1.77	1.70
Tm	0.55	0.45	0.78	0.48	0.58	0.33	0.33	0.26	0.25
Yb	3.81	3.10	5.43	3.24	3.88	2.07	2.02	1.71	1.72
Lu	0.59	0.49	0.86	0.52	0.61	0.29	0.29	0.26	0.27
Rb/Sr	2.94	2.88	2.71	1.32	0.95				
Rb/Ba	0.39	0.36	0.37	0.29	0.26				
K/Nb	3732	3868	4160	2526	2290				
Rb/Nb	19.41	24.84	22.11	14.93	13.34				
Nb/Ta	5.52	6.68	4.62	6.17	7.54				
K/Rb	192	155	188	169	171				
∑REE	154.66	140.1	146.57	152.71	170.82				
LREE/HREE	6.23	6.95	4.59	7.26	6.66				
Eu*	0.39	0.52	0.33	0.49	0.45	(Note: Eu* denotes the value of Eu anomaly.)			
$(La/Yb)_N$	5.70	6.88	3.76	7.18	6.43				

Then they were used for microscope, CL imaging and LA-ICP-MS analyses. Selection of zircon for the LA-ICP-MS analyses was done on the basis of the CL images. The CL investigation was performed on a scanning electron microscope at the Electron Microscope Unit, Ion Probe Center of Beijing, Institute of Geology, Chinese Academy of Geological Sciences. Trace elements and U-Pb isotopic analyses of zircon were performed on the Elan6100DRC Laser-Ablation-ICP-MS coupled to a ComPex102 Excimer 193 nm ArF laser and MicroLas GeoLas 200M optics at the Key Laboratory of Continental Dynamics of the Ministry of Education, Northwest University, Xi'an, China. The synthetic silicate glass NIST610 was used to keep the instrument in good condition, and the He stream was used to transport the aerosol into the ICP-MS where masthe ases were analyzed. The way to analyze the samples was blation of single spots, 30 μm wide and 20 to 40 μm deep, and the data were acquired in the peak-jumping-pulse-counting mode with one-point measured per peak. The zircon 91500 was used as the external calibration standard. We measured zircon 91500 after every finishing analysis of 4 or 5 spots in order to keep the instrument in complete agreement conditions during measurements of the standard and samples. The NIST SRM610 had been measured twice before and after analyzing around 20 samples, and ^{29}Si was used as an internal standard for U, Th and Pb analyses. The isotopic ratios and element contents of the zircon samples were calculated using the GLITTER (ver. 4.0, Macquarie University). The concordia ages and diagrams were obtained using the oplot/Ex (ver. 2.94) (Ludwing, 1991). The common lead was corrected with the LAM-ICPMS Common Lead Correction (ver. 3.15), following the method given by Andersen (2002). Detailed descriptions of the instrument, working parameters and calibration procedures are given by Yuan et al. (2003).

4 Petrological Geochemistry

4.1 Major elements

The major element analyses for the granite are listed in Table 1. The content of SiO_2 in the Shicaogou granite ranges from 71.81% to 73.89%, Al_2O_3 from 13.28% to 14.11%, K_2O 2.61% to 4.13%, Na_2O 2.85% to 3.78%, CaO 1.57% to 2.44% (Table 1), and all samples fall in the granitoid field on the P-Q diagram (Fig. 2a). The rock generally shows the characteristics of high contents of silicon (SiO_2>71%), aluminium (Al_2O_3>13%) and alkali (Na_2O+K_2O=6.28%–7.33%), and K_2O and Na_2O are

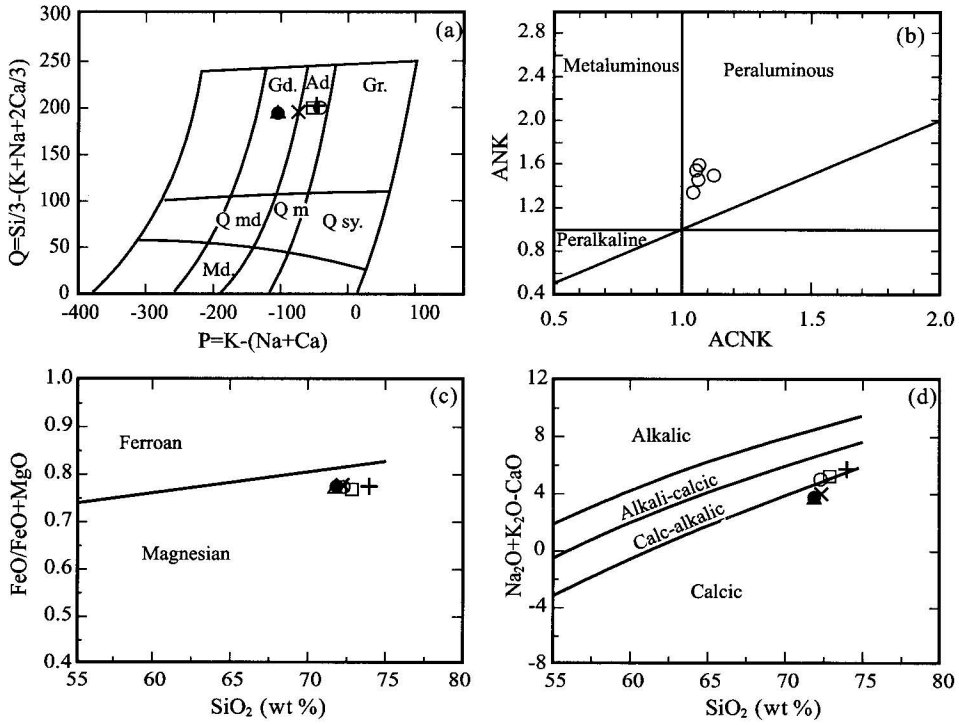

Fig. 2. Geological parameters of the Shicaogou granite plotted in various classification diagrams.

(a) P-Q diagram after Debon and Le Fort (1982), Gr – granite; Ad – adamellite (monzogranite); Gd – granodiorite; Qmd – quartz monzodiorite; Qm – quartz monzonite; Qsy – quartz syenite; (b) ANK-ACNK diagram; (c) FeO/(FeO+MgO) vs SiO_2 diagram after Frost et al. (2001); (d) Na_2O+K_2O-CaO vs SiO_2 diagram after Frost et al. (2001).

almost the same in weight (K_2O/Na_2O =0.71–1.45, with an average of 1.02). The Fe-number (FeO/FeO+MgO) varies from 0.71 to 0.76, the alkali-lime index (MALI) (K_2O+Na_2O-CaO) from 3.84 to 5.76 and the aluminum saturation index (ASI) [Al/(Ca-1.67P+Na+K)] from 1.06 to 1.13. Therefore it can be defined as a magnesian, calcic to calc-alkalic and peraluminous granite characteristic of the S-type granite (Fig. 2b, c and d), based on the latest geochemical classification for granitoids (Frost et al., 2001).

4.2 Trace elements and REEs

The contents of Rb and Sr vary from 126.2 mg/g to 205.7 μg/g and from 60.7 μg/g to 132 μg/g, respectively, and the Rb/Sr ratios from 1.32 to 2.94 (except for the 02Q-28 which has a value of 0.95). The contents of Nb (7.22 μg/g –9.5 μg/g), Ta (1.25 μg/g–1.66 μg/g) and the ratios of Nb/Ta (4.62–7.54) in the Shicaogou granite are very similar to those of crustal rocks (Nb: 8 μg/g –11.5± 2.6 μg/g, Ta: 0.7 μg/g–0.92±0.12 μg/g, and Nb/Ta: 12–13, Barth et al., 2000) and the typical continent-continent syn-collisional granites (6 μg/g –16 μg/g, 0.6 μg/g –2.6 μg/g and 6.5–10, respectively, Pearce et al., 1984). All the samples fall in the lower left field of the average values of crustal rocks on the Nb/Ta-Nb diagram, suggesting that the Shicaogou granite was derived from the melting of crustal rocks. In addition, the ratio of LILE/HFSE is one of the important tracers for a magmatic source (Hildreth et al., 1991). The Rb/Nb and K/Rb ratios are very low in mantle rocks (0.24–0.89 and 249–349, respectively, Sun and Mcdonough, 1989; Rudnick and Fountain, 1995) but high in crustal rocks (5.36–6.55 and 1433–1705, respectively). The Rb/Nb ratios of 13.34–24.84 and K/Nb ratios of 2291–4161 in the Shicaogou granite are much higher than those of crustal rocks (5–36 and 1498–2976, Rudnick and Fountain, 1995), indicating that the Shicaogou granite have resulted from the melting of crustal rocks.

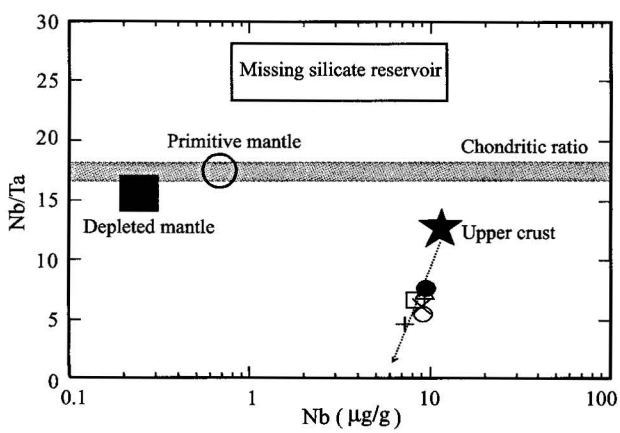

Fig. 3. Nb/Ta-Nb diagram of the Shicaogou granite.

The Shicaogou granite has a relative high total REE abundance ranging from 140.1 μg/g to 154.66 μg/g, (Table 2), and displays right-declined REE patterns with higher fractionations of LREE and HREE (LREE/HREE=4.59–7.26) and pronounced negative Eu anomalies (δEu=0.33–0.52) on the chondrite-normalized REE diagrams (Fig. 4a), suggesting a typical crust-derived granite. It is obviously rich in LILE of Rb and Th, with moderate K and Ba, and poor in HSFE of Nb, Zr, Hf, Y and Yb, exhibiting almost the same patterns of the typical continent-continent syn-collisional granite (Pearce et al., 1984) on the ocean-ridge granite normalized spider diagram (Fig. 4b). Moreover, all the samples fall within the syn-collisional granite field on the diagrams of Ta-SiO_2 and R_1-R_2 (Fig. 4c and d).

5 LA-ICP-MS Zircon U-Pb Dating

5.1 Morphology and Internal texture of zircon

The CL imaging of zircon is largely based on the genesis and contents of trace elements, especially U, Th and REE of zircon (Hanchar and Rudnick, 1995; Vavra et al., 1996, 1999; Schaltegger et al., 1999; Hermann et al., 2001). the selection of zircon grains for the LA-ICP-MS U-Pb dating in this study was done on the basis of the CL images (Fig. 5). CL investigations reveal that the zircon grains from the Shicaogou granite are generally colorless, transparent and long prismatic euhedral crystals (150–250 μm in length and 50–80 μm in width), mostly with oscillatory zoning (Fig. 5), and residual cores of irregular zircon could be found in some of enhedral zircon grains (Fig. 5d). These features reflect that the zircon was generated in magma. In addition, bright rims of different widths can be observed around the oscillatory zones (Fig. 5a and c), which may be the accretionary rims during later metamorphism.

5.2 Trace elements in zircon

The results of trace element analyses of the zircon grains from the Shicaogou granite are shown in Table 3. We can seen from the table that the contents of P, Y, Hf, Th and U are very high with wide ranges, in which P ranges from 421 μg/g to 1113 μg/g, Y from 1069 μg/g to 3341 μg/g, Hf 988 μg/g to 13966 μg/g, Th 85 μg/g to 294 μg/g, U 354 μg/g to 923 μg/g, and the Th/U ratio is between 0.14 and 0.71. All these display the features of a typical magmatic zircon (Hermann et al, 1990; Barbey et al., 1995 ; Vavra et al., 1996; Rubatto et al., 1999; Belousova et al., 2002; Hidaka et al., 2002; Rubatto, 2002).

Zircon grains from the rock have very high REE and HREE abundances, ranging from 866 μg/g to 2342 μg/g and from 774 μg/g to 2326 μg/g, respectively. All the samples display the REE patterns with depletion in LREE

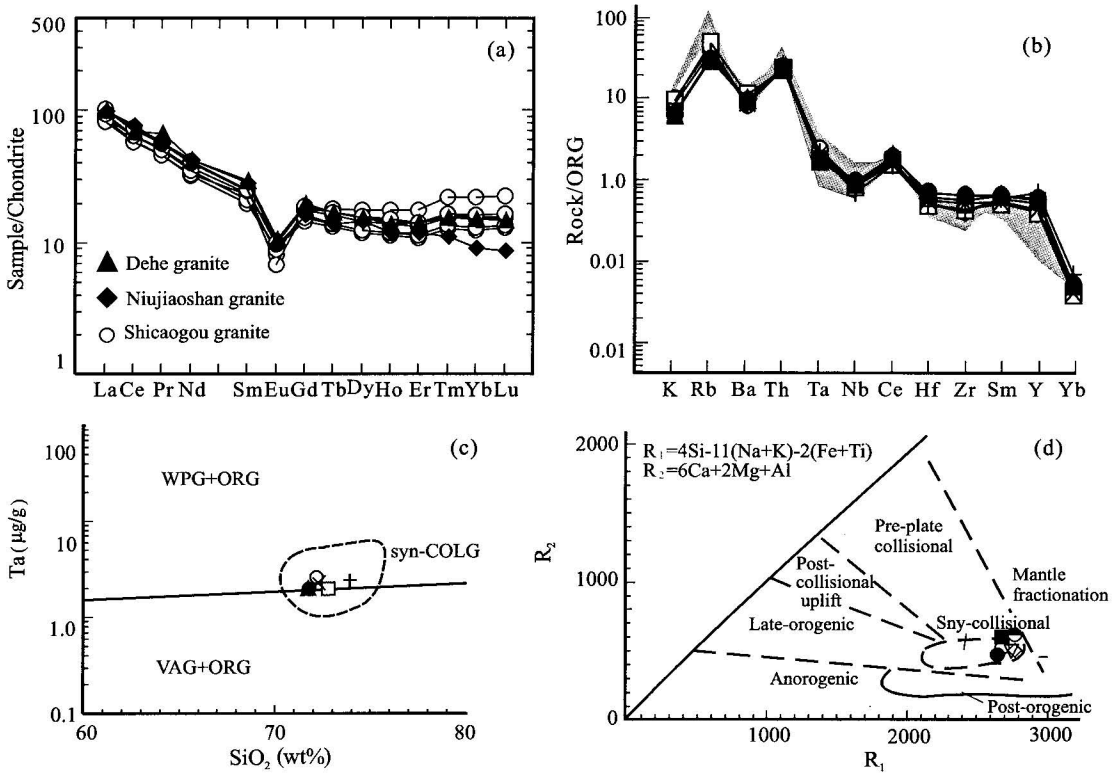

Fig. 4. Chondrite-normalized REE patterns (a), ocean ridge granite-normalized spider diagram (b) and tectonic setting diagrams (c and d) for the Shicaogou granite.

(b) The area in shadow is the typical continent-continent syn-collisional granite field according to Pearce et al., 1984; (c) Ta vs SiO_2 diagram according to Pearce et al. 1984; (d) R_1-R_2 diagram according to Batchelor et al. , 1985.

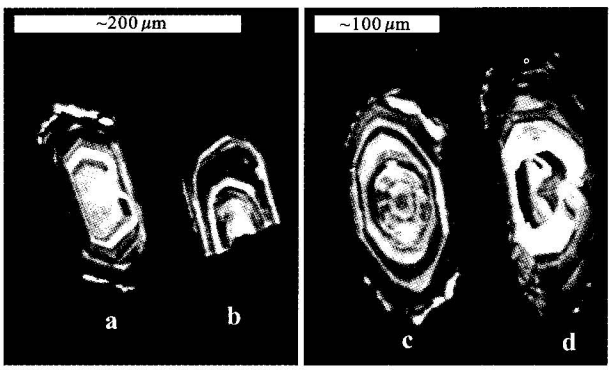

Fig. 5. CL images of zircon grains from the Shicaogou granite.

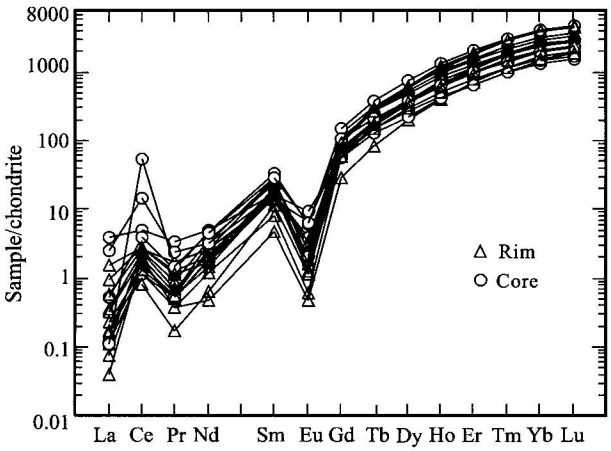

Fig. 6. Chondrite-normalized REE patterns of zircon grains from the Shicaogou granite.

and strong enrichment in HREE, and show pronounced positive Ce anomalies and negative Eu anomalies (δCe=1.42–67.74, δEu=0.01–0.25; Fig. 6). This agrees well with typical magmatic zircons (Hidaka et al., 2002; Rubatto, 2002; Whitehouse and Platt, 2003).

5.3 U-Pb zircon dating

The U-Th-Pb data from 24 spots of 19 grains were given in Table 4. We can see from Fig. 7 that all the data spread along the concordant line or adjacent areas, in which 20 spots are concentrated in a small area, and yield an average weighted $^{206}Pb/^{238}U$ age of 925±11 (2σ) Ma. Considering also the CL images, all the 20 spots fall into the magmatic domain, with high U contents (306–816 μg/g with an average of 589 μg/g) and high Th/U ratios (0.18–0.56), and thus the age 925±11 Ma represents the formation age of the

Table 3 Trace element compositions (μg/g) of the zircon grains from the Shicaogou granite

	Q24-1r	Q24-1c	Q24-2r	Q24-2r	Q24-3r	Q24-3c	Q24-4r	Q24-5r	Q24-5c	Q24-6r	Q24-6c	Q24-7r	Q24-7c	Q24-8r	Q24-8c	Q24-8	Q24-9c	Q24-9r
Y	1709	1865	1069	1080	2376	2637	2199	3046	3341	1702	1194	1773	1085	2959	1762	3033	1354	1707
Nb	1.17	1.35	1.46	1.29	3.24	1.12	0.85	1.69	2.06	1.45	0.82	1.98	1.61	2.38	3.05	2.98	0.69	0.92
La	0.062	1.46	0.124	<0.000	0.042	0.015	0.029	0.066	0.197	0.223	0.044	0.133	0.96	0.582	0.043	0.357	<0.000	0.088
Ce	1.20	5.02	1.95	1.31	2.46	1.97	1.52	1.65	3.82	2.66	1.12	2.36	14.61	2.78	53.96	2.68	0.83	1.35
Pr	0.052	0.468	0.053	0.0143	0.126	0.087	0.079	0.070	0.187	0.239	0.075	0.099	0.332	0.166	0.212	0.176	0.024	0.079
Nd	0.33	3.71	0.36	0.40	2.56	2.32	1.98	1.38	3.41	1.98	1.38	1.59	2.34	1.25	3.31	1.55	0.48	1.09
Sm	1.94	4.03	1.14	0.82	5.50	6.59	6.12	4.81	7.98	3.23	3.39	4.17	3.78	3.52	6.92	3.77	2.65	4.03
Eu	0.056	0.350	0.044	0.017	0.222	0.171	0.229	0.146	0.550	0.584	0.187	0.114	0.830	0.296	0.571	0.306	0.102	0.148
Gd	18.68	23.36	9.03	8.61	35.35	40.32	35.13	32.02	47.65	24.35	21.28	25.03	17.98	29.25	33.76	30.07	18.46	23.19
Tb	9.80	10.78	4.96	5.05	16.36	18.43	15.77	17.44	22.14	11.18	9.14	11.68	7.61	15.95	12.66	16.44	8.97	10.62
Dy	135.9	151.9	80.1	78.6	208.4	236.5	193.2	244.4	290.7	143.1	106.9	156.1	87.7	228.0	152.0	238.0	116.0	139.6
Ho	58.83	64.85	35.47	35.40	84.40	91.53	75.63	102.70	115.25	57.39	39.07	60.33	36.31	99.04	57.58	104.51	44.42	55.14
Er	281.4	299.8	178.5	183.7	375.8	406.7	330.0	484.0	524.1	255.8	167.5	261.4	164.0	468.8	255.4	492.9	197.5	250.4
Tm	64.4	69.0	42.8	46.0	81.6	88.6	69.7	106.0	110.1	55.8	36.1	56.8	37.1	105.7	52.6	109.7	42.2	55.1
Yb	625.9	676.9	435.7	468.52	758.6	826.6	653.4	1015.9	1033.1	534.4	334.7	538.8	378.3	1008.4	499.0	1043.3	394.4	523.8
Lu	111.5	114.7	75.9	84.1	132.2	142.8	114.4	178.9	183.3	96.2	59.5	91.3	66.8	177.7	89.0	183.9	72.3	95.3
Hf	12442	12088	13338	13966	11259	11488	11875	12675	11543	12580	12678	10918	10881	12658	9632	12785	12711	13920
Ta	1.00	1.06	1.28	1.89	1.00	0.73	0.56	0.97	0.99	1.17	0.58	1.12	0.55	1.65	0.88	1.59	0.59	1.05
Th	90.6	95.2	64.7	59.2	193.6	189.6	107.6	162.1	331.6	133.2	74.5	164.3	130.3	241.1	346.5	248.0	58.8	83.1
U	409.0	414.4	397.6	478.7	491.1	473.3	352.4	663.9	699.9	580.4	348.9	500.8	241.6	988.9	257.3	988.4	350.6	434.0
Th/U	0.22	0.23	0.16	0.12	0.39	0.40	0.31	0.24	0.47	0.23	0.21	0.33	0.54	0.24	1.35	0.25	0.17	0.19
Nb/Ta	1.17	1.27	1.14	0.68	3.24	1.54	1.52	1.74	2.08	1.24	1.42	1.77	2.92	1.44	3.47	1.87	1.16	0.88
EREE	1311	1426	866	913	1704	1863	1497	2189	2342	1187	780	1210	819	2141	1217	2228	898	1160
Ce*	4.57	1.42	5.62	26.23	4.97	6.09	4.84	4.99	4.20	2.36	3.51	4.55	6.06	2.08	67.74	2.48	9.85	3.46
Eu*	0.02	0.09	0.03	0.01	0.04	0.02	0.04	0.03	0.07	0.14	0.05	0.03	0.25	0.06	0.09	0.06	0.03	0.04

Note: Ce* and Eu* denote the values of Ce and Eu anomalies.

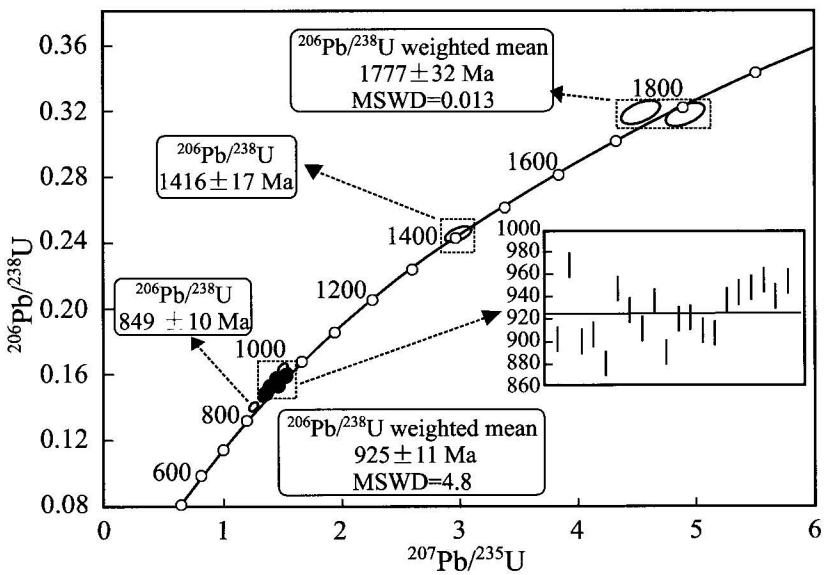

Fig. 7. Concordia diagram showing LA-ICP-MS U-Pb data for zircon from the Shicaogou granite.

Shicaogou granite. In addition, two spots (Q24-10.1 and Q24-11) from the residual cores distributed on the concordant line give an average weighted age of 1777±32 Ma, representing the protolith age of the granite. Another spot (Q24-6.1) on the concordant line between the two age areas gives an age of 1416±17 Ma, which may be the mixture age of the magmatic domain and the residual core and may be of little geological significance. Moreover, a spot (Q24-2) very close to the concordant line below the age concentration area gives an age of 849±10 Ma, which may represent the mixture of later metamorphic events.

Table 4 LA-ICP-MS U-Th-Pb data for zircon from the Shicaogou granite

				Isotopic ratios								Age (Ma)							
	^{232}Th	^{238}U	Th/U	$^{207}Pb/^{206}Pb$	1σ	$^{206}Pb/^{238}U$	1σ	$^{207}Pb/^{235}U$	1σ	$^{208}Pb/^{232}Th$	1σ	$^{207}Pb/^{206}Pb$	1σ	$^{206}Pb/^{238}U$	1σ	$^{207}Pb/^{235}U$	1σ	$^{208}Pb/^{232}Th$	1σ
24-1	128.21	568.71	0.23	0.0661	0.0017	0.15026	0.00201	1.3680	0.0344	0.04606	0.00115	810	51.9	902	11.3	875	14.8	910.2	22.2
24-2	105.69	698.53	0.15	0.0649	0.0014	0.14078	0.0018	1.2582	0.02691	0.04625	0.00111	771	44.0	849	10.2	827	12.1	913.8	21.5
24-2.1	104.51	522.53	0.20	0.0668	0.0013	0.16348	0.00208	1.5036	0.0302	0.04698	0.00098	831	40.7	976	11.5	932	12.2	927.9	18.9
24-3	78.02	359.68	0.22	0.0692	0.0016	0.14996	0.00198	1.4281	0.0336	0.04603	0.00109	903	47.7	901	11.1	901	14.1	909.6	21.1
24-4	157.5	624.61	0.25	0.0657	0.0012	0.15115	0.0019	1.3667	0.0264	0.04032	0.00074	796	39.2	907	10.7	875	11.3	799	14.5
24-5	274.28	721.28	0.38	0.0669	0.0012	0.14662	0.00184	1.3512	0.0257	0.04129	0.00064	835	38.3	882	10.4	868	11.1	817.9	12.5
24-6	134.74	663.29	0.20	0.0661	0.0012	0.15829	0.00198	1.4412	0.0262	0.04249	0.00079	810	36.6	947	11.0	906	10.9	841	15.3
24-6.1	263.91	330.67	0.80	0.0881	0.0019	0.24572	0.00326	2.9803	0.0632	0.06784	0.00099	1384	39.8	1416	16.9	1403	16.1	1326.7	18.7
24-7	153.69	680.63	0.23	0.0666	0.0012	0.15485	0.00194	1.4211	0.0262	0.03984	0.00072	826	37.0	928	10.8	898	11.0	789.7	14.1
24-7.1	210.99	718.43	0.29	0.0698	0.0013	0.15204	0.00192	1.4625	0.0277	0.03264	0.00056	924	37.5	912	10.8	915	11.4	649.1	10.9
24-8	118.66	536.70	0.22	0.0694	0.0014	0.15625	0.00201	1.4933	0.0308	0.0453	0.00092	910	41.3	936	11.2	928	12.6	895.4	17.8
24-9	222.00	632.05	0.35	0.0677	0.0017	0.14826	0.00198	1.3819	0.0339	0.03886	0.00076	858	50.1	891	11.1	881	14.5	770.7	14.9
24-10	146.97	573.15	0.26	0.0660	0.0015	0.15357	0.00201	1.3959	0.0316	0.03947	0.00081	806	46.3	921	11.2	887	13.4	782.5	15.8
24-10.1	85.02	135.04	0.63	0.1127	0.0026	0.31703	0.00449	4.9231	0.1128	0.0916	0.0017	1844	40.9	1775	22.0	1806	19.3	1771.5	31.4
24-11	83.77	110.19	0.76	0.1035	0.0027	0.31777	0.00464	4.5300	0.1155	0.08202	0.00161	1687	46.5	1779	22.7	1737	21.2	1593.3	30.0
24-12	157.76	676.61	0.23	0.0675	0.0012	0.15375	0.00194	1.4297	0.0268	0.04364	0.00079	853	37.2	922	10.9	901	11.2	863.3	15.4
24-13	150.01	680.78	0.22	0.068	0.0013	0.15171	0.00193	1.4300	0.0278	0.04209	0.0008	881	38.6	911	10.8	902	11.6	833.3	15.4
24-14	149.35	787.36	0.19	0.0693	0.0016	0.15119	0.002	1.4440	0.0331	0.0462	0.00109	908	46.1	908	11.2	907	13.8	912.8	21.1
24-15	128.32	650.32	0.20	0.0676	0.0012	0.15642	0.00198	1.4566	0.0271	0.04355	0.0008	855	36.9	937	11.0	913	11.2	861.7	15.6
24-15.1	179.14	643.58	0.28	0.0696	0.0013	0.1578	0.00202	1.5138	0.0296	0.04308	0.00075	917	38.6	945	11.2	936	11.9	852.5	14.6
24-16	170.29	306.16	0.56	0.0696	0.0017	0.15841	0.00214	1.5197	0.0379	0.04253	0.00075	917	50.2	948	11.9	938	15.3	841.8	14.6
24-17	118.08	404.12	0.29	0.0688	0.0015	0.15985	0.00209	1.5161	0.0333	0.04178	0.00082	893	44.0	956	11.6	937	13.4	827.3	16.0
24-18 c	220.84	484.5	0.46	0.0682	0.0015	0.15706	0.00207	1.4757	0.0330	0.04178	0.0007	873	45.0	940	11.5	920	13.6	827.3	13.7
24-19	147.62	815.73	0.18	0.0682	0.0012	0.15956	0.00202	1.5007	0.0275	0.04249	0.00081	875	36.0	954	11.2	931	11.1	841	15.7

6 Conclusion and Discussion

Geochemical studies of the Shicaogou gneissoid granite suggest that the rock displays the characteristics of a magnesian, calcic to calc-alkalicand peraluminous granite of the crust-origin, continent-continent syn-collisional S-type.

CL investigations and trace element data have revealed that zircon grains from the Shicaogou granite are generally typical zircon growing in magma. Residual cores of irregular zircon could be found in a few enhedral grains, and the bright rims of different widths may be the products of later metamorphism. The LA-ICP-MS U-Pb isotopic data from 24 spots of 19 zircon grains demonstrate that 20 spots in the oscillatory microzone yield an average weighted $^{206}Pb/^{238}U$ age of 925±11 Ma, indicating that the Shicaogou granite was formed in the Neoproterozoic. Two spots at the residual cores give a residual protolith age of 1777±32 Ma. The age is consistent with that of the Qinling Group within tolerance (Liu et al., 1993; Zhang Zongqing et al., 1994; Zhang Guowei et al., 2001; Zhang Benren et al., 2002), implying that the Shicaogou granite may be a product of the remelting of rocks of the Qinling Group.

Compared with other Neoproterozoic syn-collisional S-type granites in this area, the Shicaogou granite studied in this paper is distributed close to the Dehe granite in spatial, similar to the Zhaigen granite in terms of petrography, and identical with the Njiujiaoshan, Dehe and Zhaigen granites in geochemical characteristics (Table 2, Fig. 4a, Wang Xiaoxia et al., 1997), thus they should be considered to be products of the same tectono-thermal event. Considering also that it has geochemical features of a typical continent-continent syn-collisional S-type granite, the obtained 925±11 Ma formation age of the Shicaogou granite can be interpreted to further indicate that collision and amalgamation events could have occurred between some continental blocks in the Qinling orogenic belt during the Neoproterozoic. This, in turn, provides an accurate chronological constraint on the Neoproterozoic break-up and convergence in the belt.

Acknowledgements

This work was supported jointly by the National Natural Science Foundation of China (Grant No. 140032010-C, 49972063), the National Key Basic Research and Development Project of China (Grant No. G1999075508),

the Ministry of Education's Teacher Fund (No. 40133020), the Natural Science Foundation of Shaanxi Province (2002D03), the Special Foundation of the Department of Education of Shaanxi Province (01JK108) and the Science Foundation of Northwest University. We appreciate Prof. Luo Jinhai, Dr. Guo Anlin and Dr. Hua Hong at the Northwest University for polishing the English, and Han Jian'en, Wang Tao and Guo Libin at the university for the field work.

Manuscript received Oct. 30, 2003
accepted Jan. 30, 2004
edited by Zhu Xiling

References

Andersen, T., 2002. Correction of common lead in U-Pb analyses that do not report ^{204}Pb. *Chemical Geology*, 192: 59–79.

Barth, M.G., McDonough, W.F., and Rndnick, R.L., 2000. Tracking the budget of Nb and Ta in the continental crust. 165: 197–213.

Batchelor, R.A., and Bowden, K.M., 1985. Petrogenetic interpretation of granitoid rock series using multicationic parameters. *Chem. Geol.*, 48: 43–55.

Belousova, E.A., Griffin, W.L,, Suzanne, Y., O'Reilly, S.Y., and Fisher, N. I., 2002. Igneous zircon: trace element composition as an indicator of source rock type. *Contrib. Mineral Petrol.*, 143: 602–622.

Debon, F., and Le Fort, P., 1982. A chemical-mineralogical classification of common plutonic rocks and associations. Trans. R. Soc. Edinburgh: *Earth Science*. 73, 135–149.

Dong, Y. P., Zhou, D. W. and Liu, L.. 1997a. Sm-Nd isotopic ages of the Songshugou ophiolite from the east Qinling and its geological significance. *Regional Geology of China*, 16(2): 217–221 (in Chinese with English abstract).

Frost, B. R., Barnes, C.G.,. Collins, W.J., Arculus, R. J., Ellis, D. J and Frost, C.D., 2001. A Geochemical classification for granitic rocks. *Journal of Petrology*, 42: 2033–2048.

Gao Shan, Ling, Wenli, Qiu, Yumin, Zhou Lian, Hartmann, G., and Simen, K., 1999. Contrasting geochemical and Sm-Nd isotopic compositions of Archean metasediments from the Kongling high-grade terrain of the Yangtze craton: Evidence for cratonic evolution and redistribution of REE during crustal anatexis. *Geochim. et Cosmochim. Acta*, 63: 2071–2088.

Hanchar, J.M., and Rudnick, R.L., 1995. Revealing hidden structures: the application of cathodoluminescence and back-scattered electron imaging to dating zircons from lower crustal zenoliths. *Lithos*, 36: 289–303.

Heaman, L.M., Bowins, R., and Crocket, J., 1990. The chemical composition of igneous zircon suits: Implications for geochemical tracer studies. *Geochim. et Cosmochim. Acta*, 54: 1597–1607.

Hermann, J., Rubatto, D., Korsakov, A. and Shatsky, V.S., 2001. Multiple zircon growth during fast exhumation of diamondiferous, deeply subducted continental crust (Kokchetav Massif, Kazakhstan). *Contrib. Mineral Petrol.*, 141: 66–82.

Hidaka, H., Shimizu, H., and Adachi, M., 2002. U-Pb geochronology and REE geochemistry of zircons from Paleoproterozoic paragneiss clasts in the Mesozoic Kamiaso conglomerate, central Japan: evidence for an Archean provenance. *Chemical Geology*, 187: 279–293.

Hildreth, W., Halliday, A.N., and Christiansen, R.L., 1991. Isotopic chemical evidence concerning the genesis and contamination of basaltic and rhyolitic magma beneath the Yellowstone Plateau volcanic field. *Journal of Petrology*. 32: 63–138.

Li Shuguang, Chen Yizhi, Zhang Guowei and Zhang Zongqing, 1991. Alps olivine body emplaced in 1000 Ma: evidence for plate regime of Late Proterozoic in Northern Qinling. *Geological Review*, 37(3): 235–242 (in Chinese with English abstract).

Meng Qingren and Zhang Guowei, 1999. Timing of collision of the North and South China blocks: Controversy and reconciliation. *Geology*, 27(1): 1–96.

Pearce, J.B., Harris, N.B.W., and Tindle, A.G., 1984. Trace element discrimination diagrams for the tectonic interpretation of granitic rocks. *Journal of Petrology*, 25(4): 959–983.

Pei Xianzhi, 1997. *Composition and Tectonic Evolution of Shangdan Fault, Eastern Qinling*. Xi'an: Publishing House of Maps, 184.

Rubatto, D., 2002. Zircon trace element geochemistry: Partitioning with garnet and the link between U–Pb ages and metamorphism. *Chemical Geology*, 184: 123–138.

Rubatto, D., Gebauer, D., and Compagnoni, R., 1999. Dating of eclogite-facies zircons: the age of Alpine metamorphism in the Sesia–Lanzo Zone (Western Alps). *Earth and Planetary Science Letters*, 167: 141–158.

Rudnick, R.L., and Fountain, D.M., 1995. Nature and composition of the continental crust: A lower crustal perspective. *Rev. Geophys.*, 33: 267–309.

Schaltegger, U., Fanning, C.M., Günther, D., Maurin, J.C., Schulmann.K., and Gebauer, D., 1999. Growth, annealing and recrystallization of zircon and preservation of monazite in high-grade metamorphism: Conventional and in-situ U-Pb isotope, cathodoluminescence and microchemical evidence. *Contrib. Mineral. Petrol.* 134: 186–201.

Sun, S.S., and McDonough, W.F., 1989. Chemical and isotopic systematics of ocean basalts: implication for mantle composition and process. In: Saunders A.D., and Norry M.J. (eds.), *Magmatism in the Ocean Basin*. Geological Society Special Publication, 3313–345.

Sun Yong, Lu Xinxiang, Han Song, Zhang Guowei and Yang Sixiang, 1996. The composition and geochemical characteristics of Proterozoic Erlangping ophiolite in northern Qinling. *Science in China* (series D), 26 (Suppl.): 49–55.

Vavra, G., Gebauer, D., Schmid, R., and Compston, W., 1996. Multiple zircon growth and recrystallization during polyphase Late Carboniferous to Triassic metamorphism in granulites of the Ivrea Zone (Southern Alps): An ion microprobe (SHRIMP) study. *Contrib. Mineral Petrol.*, 122: 337–358.

Vavra, G., Schmid, R., and Gebauer, D., 1999. Internal morphology, habit and U-Th-Pb microanalysis of amphibolite-to-granulite facies zircons: Geochronology of the Ivrea Zone (Southern Alps). *Contrib. Mineral Petrol.*, 134:380–404.

Wang Xiaoxia, Wang Tao and Li Wuping, 1997. The geochemical characteristics and genesis of the granitic gneisses in Qinling complex. *Journal of Mineralogy and Petrology*. 17(3): 76–82 (in Chinese with English abstract).

Wang Tao, Wang Xiaoxia and Li Wuping, 1998. U-Pb isotopic

age of granitic gneisses from core complex of Qinling orogeny and its geological significance. *Regional Geology of China*, 17 (3): 262–265 (in Chinese with English abstract).

Wang Tao, Zhang Guowei, Pei Xianzhi, Zhang Chengli and Li Wuping, 2002. possibility of the existence of a Neoproterozoic NW trending orogenic belt in the North Qinling and convergence and breakup of blocks on its two sides. *Chinese Geological Bulletin*, 21(8–9): 516–522 (in Chinese with English abstract).

Whitehouse, M.J., and Platt, J.P., 2003. Dating high-grade metamorphism-constraints from rare-earth elements in zircon and garnet. *Contrib. Mineral Petrol.*, 145: 61–74.

Yang Jingsui, Xu Zhiqin, Pei Xianzhi, Wu Cailai, Zhang Jianxin, Li Haibing, Meng Fancong and Rong He, 2002. Discovery of diamond in North Qinling: Evidence for a giant UHPM belt across central China and recongnition of Paleozoic and Mesozoic dual deep subduction between North China and Yangtze plates. *Acta Geologica Sinica* (English edition), 76(4): 484–495.

Yuan Honglin, Wu Fuyuan, Gao Shan, Liu Xiaoming, Xu Ping and Sun Deyou, 2003. LA-ICP-MS U-Pb dating and rare earth element analysis of zircons from a Cenozoic intrusive in Northeast China. *Chinese Science Bulletin*, 48: 1511–1520 (in Chinese).

You Zhendong, Suo Shutian, Han Yujing, Zhang Zongqing and Chen Nengsong, 1993. *The Metamorphic Processes and Tectonic Analyses in the Core Complex of an Orogenic Belt: An Example from Eastern Qinling Mountains*. Wuhan: China University of Geosciences Press, 202 (in Chinese).

Zhang Benren, Gao Shan, Zhang Hongfei, Han Yinwen et al., 2002. Geochemistry of *Qinling Orogenic Belt*. Beijing: Science Press, 49–86 (in Chinese).

Zhang Guowei, Zhang Benren, Yuan Xuecheng and Xiao Qinghui, 2001. *Qinling Orogenic Belt and Continental Dynamics*. Beijing: Science Press, 855 (in Chinese).

Zhang Hongfei, Zhang Benren and Luo Tingchuan, 1993. Geochemical study of genesis and tectonic setting for Late proterozoic granitoids, north Qinling, China. *Earth Science—Journal of China University of Geosciences*. 18(2): 194–202 (in Chinese with English abstract).

Zhang Zongqing, Liu Dunyi and Fu Guomin, 1994. *Study on the isotopic chronology of metamorphic strata in North Qinling*. Beijing: Geological Publishing House, 76 (in Chinese).

Zhang Zongqing, Zhang Guowei and Tang Suohan, 2002. *Isotopic Chronology of Metamorphic Strata in South Qinling*. Beijing: Geological Publishing House, 196–199 (in Chinese).

Zhou Dingwu, Liu Liang, Hua Hong and Dong Yunpeng, 1996. The middle and late Proterozoic geological evolution of north Qinling with discussion on some related problems. *Geological Journal of Universities*, 2(2):166–175 (in Chinese with English abstract).